# Impact of Cumulus Cloud Spacing on Landsat Atmospheric Correction and Aerosol Retrieval

GUOYONG WEN[1]
ROBERT F. CAHALAN[2], SI-CHEE TSAY[2], AND LAZAROS OREOPOULOS[1]

*Journal of Geophysical Research (Atmospheres)*

[1] Joint Center for Earth Systems Technology, U. of Maryland Baltimore County, Maryland.
[2] NASA Goddard Space Flight Center, Greenbelt, Maryland.
Corresponding author address:
Guoyong Wen
NASA/GSFC, Code 913
Greenbelt, MD 20771

**Authors -** Dr. Guoyong Wen

Joint Center for Earth Systems Technology

The University of Maryland Baltimore County

1000 Hilltop Circle

Baltimore County, MD 21250

(301) 614-6220 (voice)

(301) 614-6307 (fax)

wen@climate.gsfc.nasa.gov

Dr. Robert F. Cahalan

NASA Goddard Space Flight Center

Code 913

Greenbelt, MD 20771

(301) 614-5390

Dr. Si-Chee Tsay

NASA Goddard Space Flight Center

Code 913

Greenbelt, MD 20771

(301) 614-6188

Dr. Lazaros Oreopoulos

Joint Center for Earth Systems Technology

University of Maryland at Baltimore County

Baltimore County, MD 21250

(301) 614-6128

## ABSTRACT

A Landsat-7 ETM+ image acquired over the Southern Great Plains DoE/ARM site during the ARESE II experiment is used to study the effect of clouds on reflected radiation in clear patches of a cumulus cloud field. The result shows that the apparent path radiance in the clear patches is enhanced by nearby clouds in both band 1 (blue) and band 3 (red) of ETM+. More importantly, the magnitude of the enhancement depends on the mean cloud-free distance in the clear patches. For cloud-free distance less than 0.5 km, the enhancement of apparent path radiance is more than 0.025 and 0.015 (reflectance units) in band 1 and band 3 respectively, which corresponds to an enhancement of apparent aerosol optical thickness of ~0.25 and ~0.15. Neglecting of the 3-D cloud effect would lead to underestimates of surface reflectance of ~0.025 and ~0.015 in the blue and red band respectively, if the true aerosol optical thickness is 0.2 and the surface reflectance is 0.05. The enhancement decreases exponentially with mean cloud-free distance, reaching asymptotic values of 0.09 for band 1 and 0.027 for band 3 at a mean cloud-free distance about 2 km. The asymptotic values are slightly larger than the mean path radiances retrieved from a completely clear region -- 0.086 and 0.024 for the blue and red band respectively.

## 1. INTRODUCTION

Modern era Earth observations from satellite platforms provide a good opportunity to remotely sense surface reflective characteristics and atmospheric properties on a global scale. Techniques have been developed to retrieve aerosol optical thickness and to correct atmospheric effects for satellite images in clear sky conditions [Kaufman et al., 1997; Wen et al., 1999]. In a clear atmosphere, solar radiative transfer may be accurately described by a plane parallel approach [Stamnes et al., 1988; Tsay et al., 1990]. However, the global average cloud cover is about 60%, so that satellite images in many geographic locations are often contaminated with clouds. Excluding cloudy scenes not only limits the usefulness of satellite measurements, but also leads to clear sky biases in retrieved atmospheric properties, since much of the clear sky near clouds is excluded.

One cloud type with interesting properties that appears frequently in satellite images is fair weather cumulus. Landsat measurements have been used to investigate the statistics of cumulus cloud fields [Wielicki and Welch, 1986; Cahalan and Joseph, 1989; Joseph and Cahalan, 1990]. High spatial resolution Landsat images are also useful for studying radiative transfer in clear patches of cumulus cloud fields. Surface features in clear patches are apparent in satellite images just by visual inspection, indicating a major contribution from the clear region itself. Therefore, it is possible to infer surface reflective characteristics and atmospheric properties even in the presence of scattered cumulus when satellite spatial resolution is sufficient to resolve cloud free gaps.

Comparing with the path radiance in a completely clear region, Cahalan et al., [2000] found that the apparent path radiance of ETM+ band 1 at 0.49 μm and band 3 at 0.66 μm for clear patches in a cumulus cloud field was significantly enhanced by nearby clouds, leading to an overestimate of aerosol optical thickness and, consequently, to an underestimate of surface reflectance. However, to quantify this

effect and link it to cumulus cloud characteristics is a great challenge because of the complex nature of cumulus clouds.

Despite cloud complexity, several fundamental questions can be addressed in studying the cloud effects on radiation in clear regions of cumulus fields. First, we would like to know to what extent clouds affect radiation in nearby clear regions. Second, we want to examine how to quantify cloud effects by looking for major factors responsible for these effects. For example, cloud effects are expected to be less pronounced when clouds are separated farther apart. Can this phenomenon be observed? Can we parameterize cloud effects in satellite images? In section 2, we present theoretical results to demonstrate the potential extent of cloud effects on downwelling irradiance at the surface. After the description of the dataset and analysis technique in sections 3 and 4, we show in section 5 the dependence of path radiance on cloud-free distance, the resulting impact on aerosol and surface retrievals, and how such retrievals can be corrected for cloud effects.

## 2. PRELIMINARIES

Cumulus clouds have a complex geometry, as we see from satellite images or our day-to-day experience. Research has shown the fractal structure of cumulus cloud fields [Cahalan and Joseph, 1989]. The description of radiative transfer in cumulus cloud fields requires a solution of the radiative transfer equation in 3-dimensional (3-D) space. Because of the complicated nature of cumulus clouds, a full description of radiative transfer as a function of cloud optical properties in a realistic, spatially extensive cumulus cloud field is not feasible at the present time. However, we may still be able to examine the upper bound of influence of clouds on nearby clear regions without complicated 3-D radiative transfer calculations.

Clouds act both as sinks and sources of solar radiation in the surface-atmosphere system. For simplicity, we shall examine the effects of clouds on the downwelling

irradiance at the surface level. As a sink, clouds reflect solar radiation away, casting shadows at the ground. As a source, clouds produce diffuse radiation, enhancing the downwelling irradiance at the surface.

Both sink and source effects of cloud can be large. It is evident that the shadowing effects reach maximum when cloud has infinitely large optical depth with sufficiently large horizontal dimensions. In this case, the surface irradiance approaches zero.

To demonstrate the magnitude of the source effect of cloud, that is the downwelling irradiance enhancement at the surface level in a clear region, we examine an idealized situation of a "hole" or clear patch in a plane-parallel cloud with an overhead sun. The hole is assumed to be small, but large enough to contain the solar disk for surface viewers directly below (the solar disk is about half degree viewed from the Earth). For simplicity, atmospheric effects (aerosol, molecular scattering and absorption) are ignored, and surface reflectance is assumed to be zero. [An example that may approximate this simplified cloud is a Karman Vortex cloud over ocean, similar to the one recently discussed by DeFelice et al. [2000] ].

The downwelling irradiance in the clear hole at the surface level is the sum of the irradiance directly through the hole ($F_0$ ) and the diffuse radiation from cloud ($F_d$ ). Since the hole is assumed to be very small, the downwelling diffuse irradiance from the cloud may be approximated by that from a plane-parallel cloud. The total transmittance of the solar irradiance at the surface underneath the clear hole may be defined as

$$T = \frac{F_0 + F_d}{F_0} \qquad (1)$$

Since the atmospheric effects are ignored, $F_0$ is the same as the solar irradiance at the top of the atmosphere. The diffuse component is calculated using the discrete-ordinate radiative transfer model [Stamnes et al., 1988; Tsay et al., 1990] with the conservative scattering C.1 phase function [Deirmendjian, 1969].

The transmittance through the clear hole at the surface level is presented as a function of cloud optical depth (Fig. 1). It is evident that the total downwelling irradiance at the surface level increases quickly with cloud optical depth, reaching a maximum of about 1.82 times that of purely clear sky at a cloud optical depth of 3, then decreasing monotonically as cloud optical depth increases.

Even though this example is highly simplified, it reveals that the basic physical mechanism of cloud effects on the irradiance in clear gaps is through the diffuse radiation generated by multiple scattering of sunlight in clouds. Though an 82% increase in downwelling irradiance is a theoretical upper bound, it implies that the enhancement of solar radiation in clear regions of a cloudy atmosphere due to cloud adjacency effects is potentially large. Furthermore, if there is an aerosol layer underneath the cloud, and/or the surface is non-black, the additional diffuse radiation from clouds impinging on aerosols and the surface can greatly enhance the reflected solar radiation at the top of the atmosphere. If cloud adjacency effects are not accounted for, the satellite observed solar radiances will be misinterpreted, leading to large errors in the aerosol optical thickness and surface reflectance retrievals.

In real cumulus cloud fields, optically dense clouds with fractal properties embedded in an optically thin atmosphere consisting of molecules and aerosols makes the effects much more complicated and interesting [Cahalan, et. al., 2000]. In the following sections, we show that such cloud effects are observable, and demonstrate that cloud spacing modulates the solar radiation reflected from clear regions of cumulus cloud fields observed by the Landsat 7 radiometer.

## 3. DATA DESCRIPTION

The Landsat 7 satellite was launched on April 15, 1999 into a sun-synchronous orbit at an altitude of 705 km. The launch of Landsat 7 continues the long-term acquisition of high spatial resolution images on global scales. Similar to its predecessor TM (Thematic Mapper) on Landsat 4 and 5, the ETM+ (Enhanced Thematic Mapper Plus) on Landsat 7 has visible (bands 1, 2, 3), near IR (band 4), and mid-IR (bands 5 and 7) bands at 30 meter spatial resolution, and a thermal infrared band at 11 μm with 60 meter resolution (band 6). In addition, the ETM+ has a new panchromatic band (band 8 at 0.52-0.9 μm) with spatial resolution of 15 meters. The improved ETM+ instrument has the ability to switch between high and low gain settings. The thermal band has both high and low gain settings operating at the same time.

A Landsat 7 ETM+ scene centered at 36.04°N, 97.87°W was acquired at 17 UTC on March 19, 2000 over the Oklahoma SGP (Southern Great Plains) site of DoE's ARM (Department of Energy's Atmospheric Radiation Measurement) program during ARESE (ARM Enhanced Shortwave Experiment) II period. The cloud cover of the 185 km × 180 km ETM+ scene is about 40 percent as shown in the gray scale image (Fig. 2). The left portion of the scene is clear with a few small isolated cumuli. An overcast stratocumulus cloud can be seen at the right part of the image. From clear to overcast, we see scattered fair weather cumulus clouds and cloud streets. As cloud cover increases from clear to overcast, the cloud spacing gradually decreases. Blowups of sub-images of 512 × 512 pixels (15 km × 15 km) from a completely clear region, and three consecutive cloudy images at the bottom show details of cloud structure.

During ARESE II, the Balloon-Borne Sounding System (BBSS) [Lesht, 1995] was launched from the central facility site at 36.6°N, 97.5°W (about 15 km east of the

rightmost sub-image in Fig. 2) every 3 hours, taking vertical profile measurements of the thermodynamic state of the atmosphere and wind speed. The Millimeter-Wavelength Cloud Radar (MMCR) [Clothiaux, et. al., 2000] and Belfort Laser Ceilometer [Turner, 1996] located at the central facility site were operating continuously to measure cloud reflectivity and to detect the cloud base.

After examining the temperature and humidity profiles (not shown) of the balloon launched at 17:28 UTC, 28 minutes after the Landsat-7 overpass, we concluded that it did not pass through clouds. However, prior temperature and humidity profiles at 11:30 UTC (not shown here) and 14:30 UTC (Fig. 3a), indicate the cloud base at 475 m and 473 m, and cloud top height of 1015 m and 860 m respectively. The cloud base heights determined from the temperature and humidity are consistent with those from BLC (not shown). The MMCR reflectivity profile also indicates the cloud base at ~0.5 km and cloud top at ~1 km above ground (Fig. 3b). Gaps in the MMCR reflectivity profile before and after the Landsat-7 overpass indicate the clear region of cumulus cloud field passing over the central facility site

We should note that the in situ profiles from the sounding, and the ground based MMCR and BCL remote measurements were made at a specific location in the 185 km × 180 km ETM+ image. Together with the in situ measurements from BBSS, the continuous measurements from MMCR and BLC indicate that clouds observed from ETM+ have cloud base about 0.5 km and cloud top height about 1 km. In this study, we focus on the cumulus cloud field between the clear region and the stratocumulus (Fig. 2).

## 4. Data Analysis

Cumulus cloud fields are complex in nature. Except for cloud shadows evident in high spatial resolution images, the effects of clouds on reflected solar radiation in

clear patches are not obvious. Even if the cloud effects can be identified, it may nevertheless be difficult to identify the major characteristics of cumulus clouds that cause these effects. In this section, we review the path radiance method, discuss identification of clouds and cloud shadows, and describe how to extract information on cloud effects from ETM+ images, and characterization of cumulus cloud fields.

## 4.1 Apparent Path Radiance

The reflected solar radiance at each pixel of an ETM+ image depends not only on the optical properties of each individual cloud but also on how they are distributed in space. The complicated cloud geometric shape and spatial distribution make it very difficult to establish a one-to-one relationship between clear sky radiance and the configuration of nearby clouds. The variable surface reflectance characteristics of land adds another difficulty in assessing the cloud effects. Therefore, it is not straightforward to isolate cloud effects from a single band of ETM+ on a pixel to pixel basis.

It has been observed that the surface reflectance at visible wavelengths (band 1 and 3 of TM and ETM+) and that at mid-IR wavelengths (band 7 of TM and ETM+) are linearly correlated over vegetation and wet soil surfaces [Kaufman et al., 1997]. The linear correlation of visible and mid-IR reflectances has been used to determine the atmospheric path radiance [Wen et al., 1999]. In an analysis of an ETM+ imagery, Cahalan et al., [2000] found that the visible and mid-IR observed reflectances are also linearly correlated in the clear gaps between cumulus clouds.

Similar to the process for the clear atmosphere [Wen et al., 1999], Cahalan et al., [2000] fitted a straight line through the lower envelope of the visible and mid-IR relations, for clear patch pixels within cumulus cloud fields. The intercept of the straight line at the zero of mid-IR reflectance, which would be close to the true path radiance if the atmosphere was completely clear, was found to be significantly

enhanced compared to that of an entirely clear region. Since the satellite-observed solar radiation is affected by nearby clouds, the intercept no longer represents the true path radiance of the clear atmosphere. The intercept therefore is defined as "apparent path radiance". Here we further demonstrate that the magnitude of the enhancement in apparent path radiance is affected by cloud spacing in the cumulus cloud field.

The visible (band 1 of ETM+) and mid-IR (band 7 of ETM+) observed reflectance relations for three sub-images (Fig. 2) of 512 × 512 pixels (or ~15 km × 15 km) from the cloudy Eastward side of the image are presented in Fig. 4, along with those from a completely clear sub-image on the Westward side. It is evident that the lower envelope of the visible and mid-IR scattered points extracted from clear regions embedded in cloudy scenes is generally higher than the completely clear sub-image as indicated by the lower straight line. The apparent path radiance determined from the intercept of zero of mid-IR of a straight line that fits through the lower envelope of the scattered relation for clear patches in cloudy region is evidently enhanced compared to the completely clear atmosphere.

The enhancement of apparent path radiance increases as cloud cover increases (or cloud spacing decreases). The enhancement of the apparent path radiance is 0.005 for the least cloudy sub-image, and 0.03 for the most cloudy sub-image. These enhancements of visible reflectance are significant. An enhancement of the path radiance about 0.005 and 0.03 will lead to an overestimate of aerosol optical thickness of 0.05 and 0.3, respectively, if a plane-parallel atmosphere is assumed [Wen et al., 1999]. An overestimate of aerosol optical thickness of 0.05 and 0.3 further leads to underestimate of surface reflectance about 0.005 and 0.03 respectively if the true aerosol optical thickness is 0.2 with surface reflectance of 0.05.

The apparent path radiance introduced here avoids the difficulty of assessing the cloud effect on the reflected solar radiation for individual pixels. Instead, it gives

the statistics of the cloud effects relative to the plane-parallel atmosphere. The apparent path radiance in clear patches of cumulus cloud fields is physically intuitive, and can be measured and compared with the path radiance in completely cloud-free regions of the same image, thus allowing determination of the impact of scattered cumulus clouds on apparent path radiance. In section 5, we present details of how cloud spacing affects the apparent path radiance.

### 4.2 CLOUD MASK

Fig. 4 of the previous section showed example that the enhancement of the apparent path radiance depends on cloud spacing in the cumulus field. Before we can further discuss cloud spacing effects on the reflected solar radiation, we need to have an accurate cloud identification scheme. A variety of techniques has been developed to identify clouds for satellite images [Coakley and Bretherton, 1982; Ackerman et al., 1998]. Landsat-7 uses the ACCA (Automated Cloud Cover Assessment) algorithm [Irish, 2000] for its acquisition strategy, but in our study there is no need to use such a complex technique. Instead, we use simple spectral discrimination to separate cloud from vegetation and bare soil background.

The reflectance of vegetation and soil depends strongly on wavelength in the solar spectrum i.e., small in visible and large in near-IR [Short, 1982], while the reflectance of clouds has less preferential dependence in those wavelengths. This is particularly true for opaque clouds (i.e., cumulus, stratocumulus, stratus clouds). We found two bands are sufficient to identify clouds for the Oklahoma scene where surface is mostly vegetated or bare soil. A visible (band 2 at 0.57μm) and a near-IR band (band 4 at 0.84 μm) are used for cloud masking.

To use the spectral information we define a unit vector composed from reflectance of two bands

$$\mathbf{P} = \frac{(r_2, r_4)}{\sqrt{r_2^2 + r_4^2}} \qquad (2)$$

where, $r_2$ and $r_4$ are observed reflectances of bands 2 and 4 of ETM+. A normalized spectral separation index (SSI) is defined to identify clouds

$$Q = \frac{\mathbf{P} \bullet \mathbf{I}}{r_2^2} \qquad (3)$$

$$\mathbf{I} = (\frac{1}{\sqrt{2}}, \frac{1}{\sqrt{2}})^{\mathrm{T}} \qquad (4)$$

where $\mathbf{I}$ is a unit vector in the 2-dimensional reflectance space. The dot product $\mathbf{P} \bullet \mathbf{I}$ measures the degree of wavelength independence of reflectance at the two bands. It ranges from 0 to 1 and takes values close to 1 when reflectances in the two bands are about equal, as for clouds. Since the surface reflectance of visible band over vegetation and bare soil is small, and cloud reflectance is relatively large for both visible and near-IR bands, the weighting factor of visible reflectance $r_2$ in the denominator of Eq. (3) makes the index $Q$ effective in separating clear from cloudy pixels.

A sub-image of 512 × 512 pixels is used to demonstrate the cloud masking process. The histogram of the $Q$ index of the sub-image (Fig. 5) clearly shows a bimodal distribution. The value of $Q$ corresponding to the minimum between the two modes ($Q_o \sim 40$) can be used as a threshold to separate cloudy from clear pixels. Pixels with $Q < Q_o$ are classified as cloudy or clear otherwise.

The distribution of $Q$ is positively skewed with a long tail towards large values. Pixels in the right tail can be shown to come mainly from cloud shadows. That is because the reflectance is wavelength dependent over shadows, and the denominator in Eq. (3) is smaller for shadows than for non-shadow pixels.

Therefore the spectral separation index $Q$ is expected to be larger for shadow pixels relative to non-shadow clear pixels.

The choice of power of 2 in the denominator in Eq. (3) comes from the following consideration. Since the numerator in Eq. (3) is less than 1 and surface reflectance is small in the visible, the greater than 1 power in the denominator makes index $Q$ much larger for clear pixels than cloudy ones. Had we used a much large power in the denominator, the behavior of the index $Q$ would have been dominated by the denominator, and the wavelength dependence information in the numerator would not have been effectively used. Therefore the power should be upper bounded in separating the clear and cloudy pixels. By visually inspecting the distribution of $Q$, we found for a power ranging from about 1.7 to 3, the index $Q$ has a bimodal distribution with different threshold values. The cloud mask result, however, is not sensitive to a specific power index in that range.

Unlike a clear bimodal distribution for clear and cloudy pixels, there is no clear cutoff for the shadows. We found that a threshold value of 150 is an appropriate cutoff value by visual examination of the shadow mask and the original image. The shadow mask is not very sensitive to the threshold value chosen. Some shadow pixels near the big cloud street are misclassified, but most clouds and shadows are captured, as can be seen in Fig. 6.

### 4.3. CLOUD-FREE DISTANCE

Strictly speaking, the radiance at each individual clear pixel in a two-dimensional image depends on the distribution of cloud and aerosol optical properties in 3-dimensional space, as well as surface reflectance. In section 4.1, we mentioned that the evaluation of the effects of cloud on reflected solar radiation on a pixel-by-pixel basis is not practical because of the complicated nature of clouds and surface reflectance. A measurable parameter, the apparent path radiance, was

introduced to quantify the cloud effects. To better understand the cloud effects physically, we now further explore the major causes of these effects.

What is needed is a parameter describing the primary statistical property of cumulus cloud fields that affects surface illumination, rather than detailed information on individual cumulus clouds. By visually inspecting the apparent path radiance and associated image, we found that the apparent path radiance depends primarily on cloud spacing. This is physically intuitive since the farther away the cloud is, the weaker the diffuse radiation from the cloud, and thus the smaller the effects.

For ideal bar clouds, or lattice cuboid clouds, the distance (edge-to-edge) between two clouds can be used to describe cloud spacing. In a real cumulus cloud field, this definition of cloud spacing is not useful. The geometry of cumulus clouds has a fractal structure [Cahalan and Joseph, 1989] with the probability distribution of cloud areas approximately following a power law [Wielicki and Welch, 1986; Cahalan and Joseph, 1989]. Because of the nature of a power-law distribution (i.e. large number of smaller clouds), the conventional edge-to-edge cloud spacing primarily represents the distance among the smaller clouds, and is thus not suitable for our purposes.

Even though cumulus cloud fields are quite complicated, they still have some special features that can be used to characterize their influence on apparent path radiance. Except for cumulus congestus, cumulus clouds have nearly flat bases at the lifting condensation level, with fairly small protuberances at the top [Cotton and Anthes, 1989]. So cloud altitude and thickness are not greatly variable in the ETM+ image. This is consistent with the in situ and ground-based measurements of clouds in this study shown earlier. Aerosol properties are also often uniform over the scale of a Landsat ETM+ image (~185km × 180km). Therefore, we primarily need a parameter that describes the cloud spacing in a 2-D field.

Since we are mainly interested in the radiation in clear patches, and the effects from nearby clouds, it is natural to link the two (i.e., to examine the statistics of distance between a clear pixel and a nearby cloud). In this study, we define the cloud-free distance of a clear pixel as the distance from the clear pixel to the closest cloud along the principal plane. The rationale for choosing the principal plane is that the sunlit parts of cumulus clouds are generally brilliant white, hence this side has the largest contribution to sunlight reflected onto the nearby surface and aerosols.

The cumulative distribution of cloud-free distances for the least cloudy sub-image is presented in Fig. 7 as an example. The mean cloud-free distance of the sub-image is 1.7 km, with standard deviation 1.9 km. It is also interesting to note that as many as half of the clear pixels have cloud spacing less than 1 km, and only the top 10th percentile of the clear pixels has a cloud-free distance larger than 4 km.

## 5. Dependence of Apparent Path Radiance on Cloud Spacing

Because the geometrical thickness of fair weather cumulus clouds is relatively constant, and aerosol properties do not vary dramatically within Landsat ETM+ images in the remote rural region of the Oklahoma ARM site, the mean cloud-free distance is expected to be a major dependence variable of cloud effects. Here, we explicitly study the relation between the observed apparent path radiance and the mean cloud-free distance.

In the analysis process, we calculated both the mean cloud-free distance and the apparent path radiance in a cloudy sub-image of 512 × 512 pixels (~15 km × 15 km). The choice of the size of the sub-image takes into consideration that the size should be much larger than typical cumulus clouds, i.e., less than 1~2 km from the power law distribution [Cahalan and Joseph, 1989]. The size should be also small enough to allow us to examine the apparent path radiance in different regions within the cumulus cloud field. In order to increase statistical significance, a moving window

of 512 × 512 pixels at an increment of 200 pixels both in horizontal and vertical is applied. Since we are interested in examining the effects of cloud on radiances of clear patches, the amount of clear pixels should be significant in any sub-image. We therefore excluded sub-images with cloud cover less than 2% or greater than 85%.

The mean cloud-free distance and apparent path radiance for both band 1 and band 3 are plotted in Fig. 8. Each point in Fig. 8 represents the mean cloud-free distance and corresponding apparent path radiance of a sub-image. The average path radiance from the clear atmosphere far away from clouds is used as a reference and plotted with a dashed line.

It is evident that the apparent path radiance is enhanced in the cumulus cloud field. The enhancement in the blue band is generally larger that that in the red band. The enhancement and associated variability increases as the mean cloud-free distance decreases for both visible bands and exceeds 0.025 and 0.015 for band 1 and band 3 respectively when the mean cloud-free distance is less than 0.5 km. The enhancement decreases to an asymptotic value at a mean cloud-free distance about 2 km. An analytical form of exponential decrease is used to parameterize the apparent path radiance and cloud-free distance relationship. The non-linear best fits for blue and red bands are:

$$r_{0.49\mu m} = 0.061 e^{-\frac{x}{0.586}} + 0.090 \qquad (5)$$

$$r_{0.66\mu m} = 0.035 e^{-\frac{x}{0.611}} + 0.027 \qquad (6)$$

where $x$ is the mean cloud-free distance in kilometers.

The path radiance in the clear atmosphere away from clouds for band 1 and band 3 is presented in Fig. 9 to examine the significance of the enhancement. The

path radiances are clustered for both blue and red bands except for several outliers. Means are 0.086 and 0.024 with standard deviation of 0.0023 and 0.0029 for band 1 and band 3 respectively excluding the top and bottom 5 percentiles. With these small standard deviations, the mean values of path radiance represent the true clear sky path radiance for both bands.

By comparing the apparent path radiance with the true path radiance and its dispersion, it is evident that the apparent path radiance is greatly enhanced for sub-images with mean cloud-free distance less than 1 km. The enhancement up to 0.025 for band 1 and 0.015 for band 3 leads to overestimates of aerosol optical thickness of 0.25 and 0.15 [Wen et al., 1999]. The overestimate in aerosol optical thickness further leads to underestimate in surface reflectance. For example, if the true aerosol optical thickness is 0.2 with the surface reflectance of 0.05, the surface reflectance will be underestimated by 0.025 and 0.015 for the two bands respectively [Wen et al., 1999]. Even with larger mean cloud-free distance, the asymtotic apparent path radiances are still systematically larger than the average true path radiance at about 1 standard deviation level.

## 6. SUMMARY AND DISCUSSION

The downwelling irradiance of solar radiation in cloud-free regions at the surface may be greatly enhanced by diffuse radiation from nearby clouds. A simple radiative transfer calculation shows that the enhancement of irradiance in a clear region could reach more than 80% at the surface. The enhanced downwelling irradiance interacting with molecules and aerosols in the atmosphere and the surface ultimately increases the reflected solar radiation. Without considering such effects, the satellite observed radiance might be misinterpreted.

Fair weather cumulus is a very common cloud type in the atmosphere. It is important to study the solar radiation transfer in clear patches of cumulus cloud

fields for both atmospheric correction and aerosol optical property retrieval in high spatial resolution satellite images. Among other factors, the reflected solar radiation is affected by the cloud spacing. In this paper, we demonstrated that the cloud effects on reflected solar radiation in clear breaks within cumulus cloud fields can be observed and quantified using the apparent path radiance which depends on cloud spacing.

Cloud effects can be observed not only using the apparent reflectance, but also parameterized by the cloud-free distance for clear pixels. Apparent path radiance is greatly enhanced when mean cloud-free distance becomes small. For a sub-image with mean cloud-free distance less than 0.5 km, the apparent path radiances are enhanced by more than 0.025 and 0.015 for the blue band and the red band respectively. These enhancements correspond to overestimates of aerosol optical thickness of ~0.25 and ~0.15, and underestimates of surface reflectance of ~0.025 and ~0.015, for the two bands respectively for plane parallel retrievals. The enhancement of the apparent path radiance decreases exponentially with mean cloud-free distance. As the mean cloud-free distance becomes larger than 2 km, the apparent path radiance approaches asymptotically 0.09 and 0.027 for the blue and red band respectively. Even though, the absolute difference between asymptotic values of apparent path radiance and the true path radiance is small, it is still statistically significant. However it also indicates that only a constant correction is needed when cloud cells are far away from each other.

The results and the technique used in this study are encouraging for further research in clear-cloudy interaction. However, they are based on an ETM+ image where the cumulus cloud appears to be uniform in vertical extent. The vertical thickness may vary from one cumulus cloud field to another (e.g., slight vertical extent for cumulus himilis and moderate vertical extent for cumulus mediocris), and hence the optical depth of clouds. Cloud microphysics also affects the optical

properties of cloud. Aerosol properties may vary from one cumulus cloud field to another. Further analysis of high spatial resolution images is needed to validate the parameterization in this study and to take into account of other factors.

*Acknowledgments*. Data were obtained from the Atmospheric Radiation Measurement (ARM) Program sponsored by the U.S. Department of Energy, Office of Science, Office of Biological and Environmental Research, Environmental Sciences Division. This research was supported by funding provided under Landsat Science Team activities, which is part of NASA-MTPE, under proposal 1996-MTPE-00116, the Department of Energy's ARM program under grants DE-A102-97ER62369 and DE-A105-90ER61069.

## REFERENCES


Ackerman, S. A., K. I. Strabala, W. P. Menzel, R. A. Frey, C. C. Moeller, and L. E. Gumley, Discrimination clear sky from clouds with MODIS, *J. Geophys. Res.*, **103**, 32,141-32,157, 1998.

Cahalan, R. F., and J. H. Joseph, Fractal Statistics of Cloud Fields, *Mon. Wea. Rev.*, **117**, 261-272, 1989.

Cahalan, R. F., L. Oreopoulos, G. Wen, A. Marshak, S.-C. Tsay, and T. DeFelice, Cloud characterization and clear sky correction from Landsat 7, *Remote Sensing of Environment,* submitted, 2000.

Clouthiaux, E.E., T. P. Ackerman, G. G. Mace, K. P. Moran, R. T. Marchand, M. A. Miller, and B. E. Martner, Objective determination of cloud heights and radar reflectivities using a combination of active remote sensor at the ARM CART sites, *J. Appl. Meteor.*, **39**, 645-665, 2000.

Coakley, J.A., and F. P. Bretherton, Cloud cover from high-resolution scanner data: detecting and allowing for partially filled fields of view, *J. Geophys. Res.*, **87**, 4917-4932, 1982.

Cotton, W. R., and R. A. Anthes, *Storm and Cloud Dynamics, Academic Press,* San Diego, Calif., 1989.

DeFelice, T. P., D. J. Meyer, G. Xian, and R. F. Cahalan, Landsat 7 reveals more than just surface features in remote area of globe, *Bull. Amer. Meteor. Soc.*, **81**, 1047-1049, 2000.

Deirmenjian, D., *Electromagnetic Scattering on Spherical Polydispersions*, Elsevier, New York 291 pp., 1969.

Irish, R., Landsat 7 Automatic Cloud Cover Assessment, Proceeding of SPIE/AeroSense 2000, Algorithms for Multispectral, Hyperspectral, and Ultraspectral Imagery VI, S. S. Shen, M. R. Descour (paper 4049-35) (in press).

Joseph, J. H., and R. F. Cahalan, Nearest-neighbor spacing of fair-weather cumulus, *J. Appl. Meteor.* **29**, 793-805, 1990.

Kaufman., Y. J., A. E. Wald, L. A. Remer, B.-C. Gao, R.-R., Li, and L. Flynn, The MODIS 2.1-μm channel correlation with visible reflectance for use in remote sensing of aerosol. *IEEE Trans. Geosci. Remote Sens.*, **35**, 1286-1298, 1997.

Lesht, B.M., An evaluation of ARM radiosonde operational performance, *Proceeding of the Ninth Symposium on Meteorological Observations and Instrumentation*, American Meteorological Society, Boston, MA., 1995.

Short, N., The Landsat Tutorial Workbook, *Basics of Satellite Remote Sensing*. NASA Ref. publ. 1078, U.S. Govt. Printing Office, Washington D.C., 1982.

Stamnes, K., S.C. Tsay, W. Wiscombe, and K. Jayaweera, Numerically stable algorithm for discrete-ordinate-method radiative transfer in multiple scattering and emitting layered media, *Appl. Opt.*, **27**, 2502-2509, 1988.

Tsay, S.-C., K. Stamnes, and K. Jayaweera, Radiative transfer in stratified atmospheres: Development and verification of a unified model, *J. Quant. Spectrosc. Radiat. Transfer*, **43**, 133-148, 1990.

Turner, D. D., Comparisons of the micropulse lidar and the Belfort Laser Ceilometer at the Atmospheric Radiation Measurement Southern Great Plains Cloud and Radiation Testbed Site, *Proceedings of the Sixth Atmospheric Radiation Measurement (ARM) Science Team Meeting*, March4-7, 1996, San Antonio, Texas.

Wielicki, B. A., and R. M. Welch, Cumulus cloud properties derived using Landsat satellite data, *J. Climate Appl. Meteor.*, **25**, 261-276, 1986.

Wen, G., S-C Tsay, R. F. Cahalan, and L. Oreopoulos, Path radiance technique for retrieving aerosol optical thickness over land, *J. Geophys. Res.*, **104**, 31,321-31,332, 1999.

FIGURE CAPTIONS

Figure 1. Transmittance at the surface level underneath small clear hole in a plane-parallel cloud as a function of cloud optical depth for overhead sun. DISORT with a C1 cloud is used to calculate the diffuse radiation. Atmospheric effects are ignored.

Figure 2. An ETM+ image acquired at 17 UTC on March 19, 2000 over the SGP ARM site in Oklahoma. Blowup sub-images show details, with a completely clear sub-image at left and three consecutive sub-images with increasing cloud cover toward the right.

Figure 3. (a) The temperature (solid) and dew point temperature (dotted) profiles ~14:30 UTC on March 19, 2000 over the ARM SGP site. The cloud base (~473 m) and top (~860 m) above the ground are indicated by solid circles. (b) The time series of Millimeter Wavelength Cloud Radar reflectivity profile above the ground at the SGP ARM site indicates cloud base and top at about 0.5 km and 1 km respectively. The timing of a Landsat-7 overpass at 17 UTC is indicated by a dashed vertical line.

Figure 4. The relation between the visible at 0.49 μm (band 1) and the mid-IR band at 2.2 μm (band 7) for the four sub-images in Fig. 2 (clear sky at left, and three cloudy sub-images in the right with different cloud fraction (CF) indicated). The intercept of zero mid-IR reflectance of a straight line that fits though the lower envelope of the visible and mid-IR relations determines the path radiance (for completely clear sky), and apparent path radiance (for clear patches in cumulus cloud field) respectively. The straight line used to determine the path radiance for clear sky (left) is also plotted in cloudy cases as a reference (lower lines).

Figure 5. The Spectral Separation Index (SSI) for a sub-image of Fig. 6 is characterized by a bimodal distribution. The mode with smaller SSI comes from cloud pixels. The clear pixels form the mode on the right. The long tail at right comes from shadow pixels. A threshold value of 40, defined by the minimum between peaks, is used to separate cloudy from clear pixels, and 150 is used as a cutoff for shadow pixels.

Figure 6. The cloud-shadow mask (right) using the SSI technique is compared with the original image (left).

Figure 7. The cumulative distribution of cloud-free distance for clear regions in the cumulus cloud field, for the sub-images in Fig. 6.

Figure 8. The apparent path radiance for ETM+ band 1 (solid circles) and band3 (open circles) as a function of mean cloud-free distance, defined in the text.

Figure 9. The path radiance for ETM+ band1 and band 3 for clear region away from cumulus cloud fields. The path radiances are clustered tightly for both bands except for several outliers. The means of the path radiances are 0.086 and 0.024, with standard deviation of 0.002 and 0.003 for band 1 and band 3, respectively, with top and bottom 5th percentile excluded.

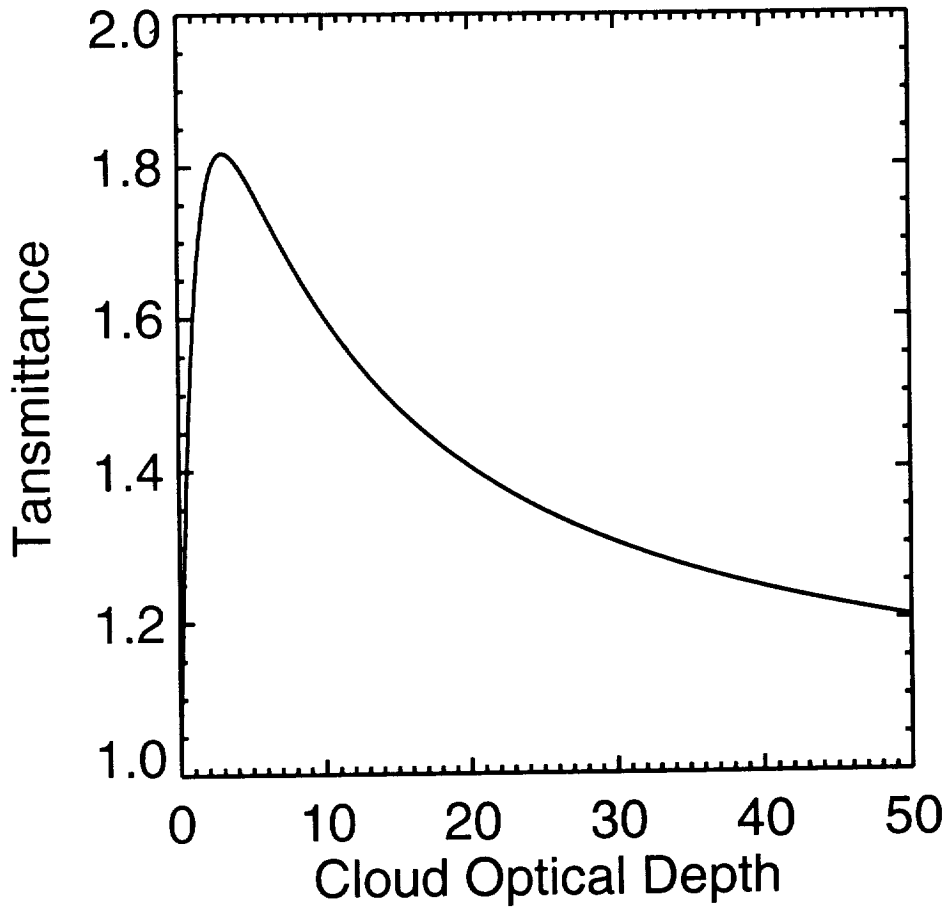
2.0
1.8
1.6
1.4
1.2
1.0
Tansmittance
0
10
20
30
40
50
Cloud Optical Depth

Fig 1

Fig. 2

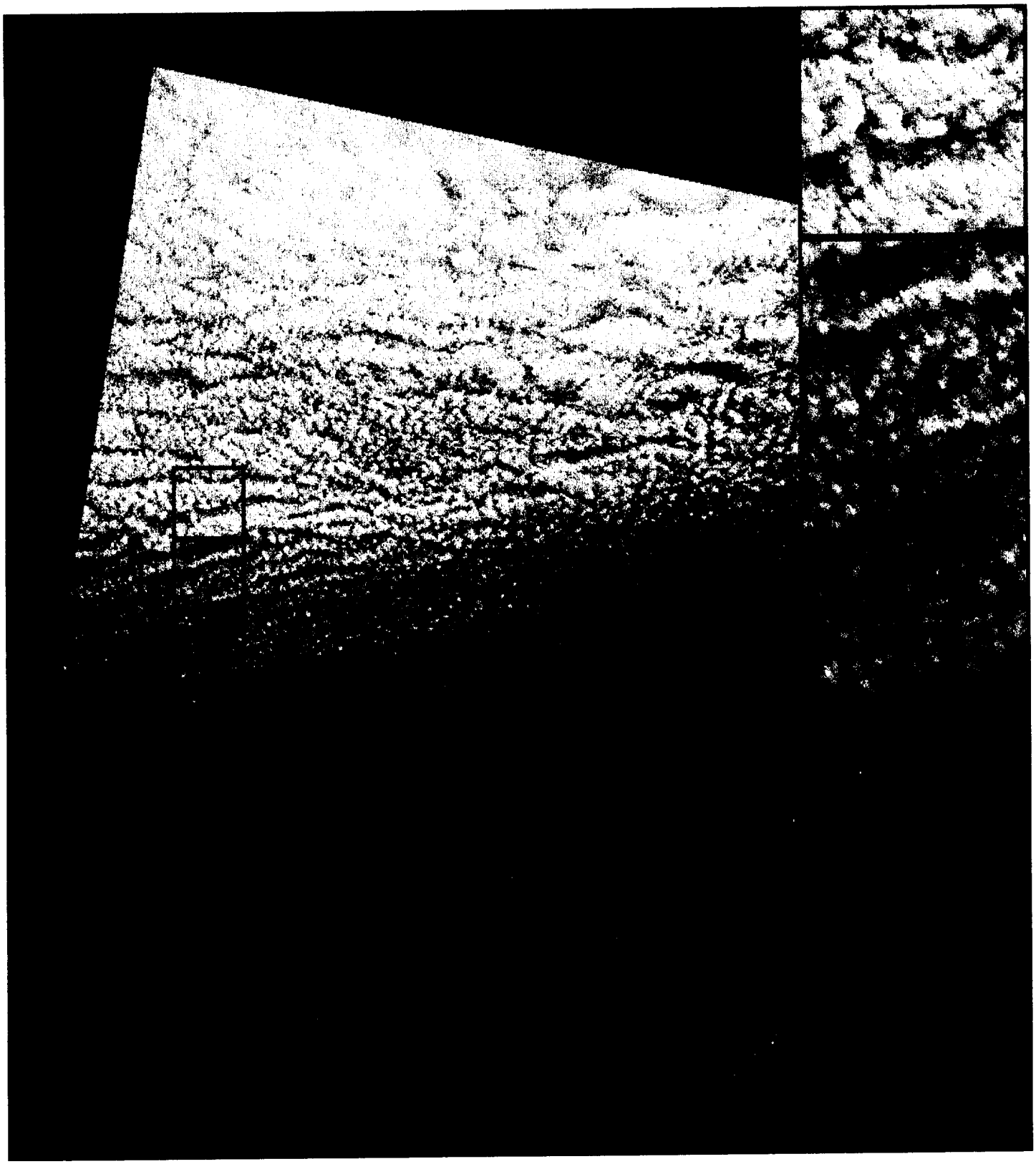

Fig. 3

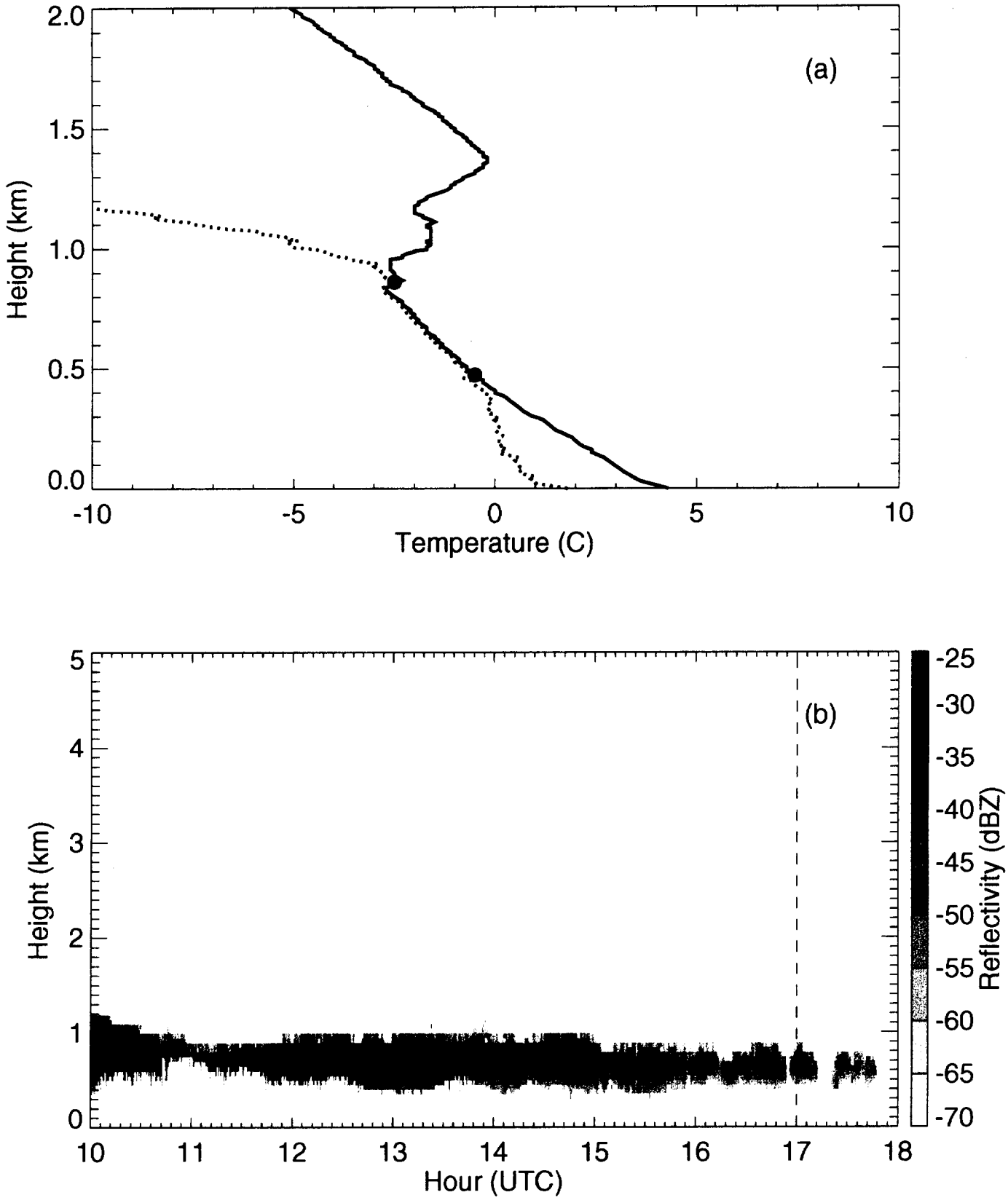
(a)
Height (km)
2.0
1.5
1.0
0.5
0.0
-10
-5
0
5
10
Temperature (C)
(b)
Height (km)
5
4
3
2
1
0
10
11
12
13
14
15
16
17
18
Hour (UTC)
-25
-30
-35
-40
-45
-50
-55
-60
-65
-70
Reflectivity (dBZ)

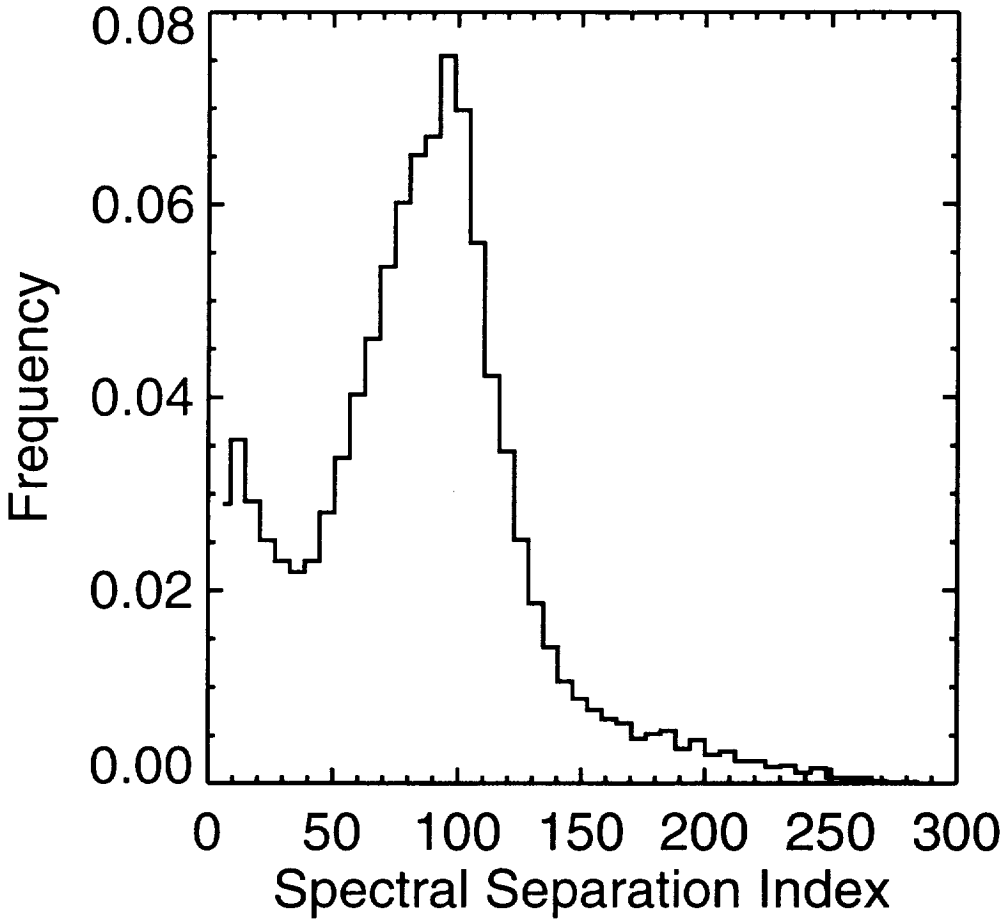
0.08
0.06
0.04
0.02
0.00
Frequency
0
50
100
150
200
250
300
Spectral Separation Index

Fig 5

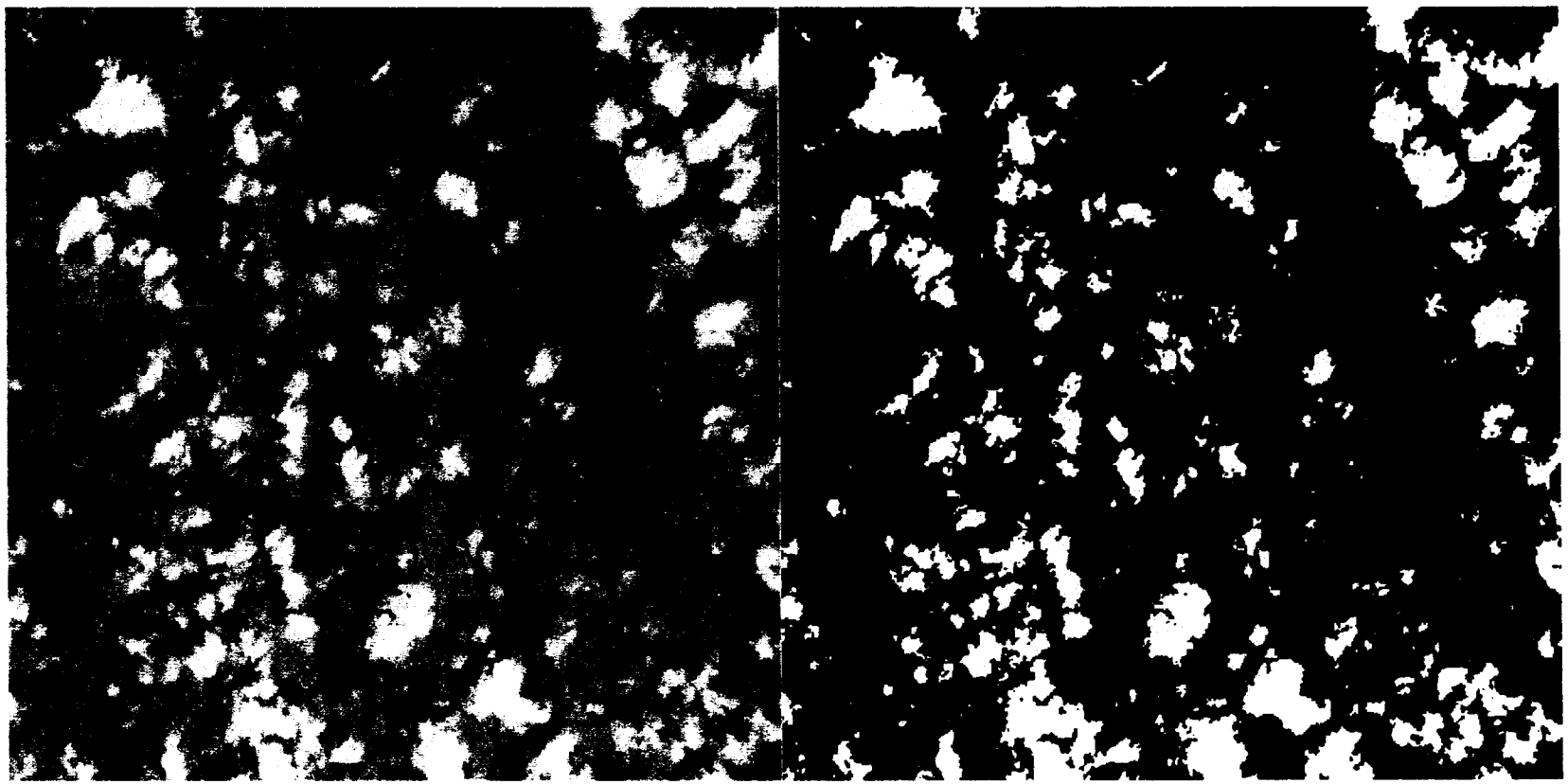

Fig 6

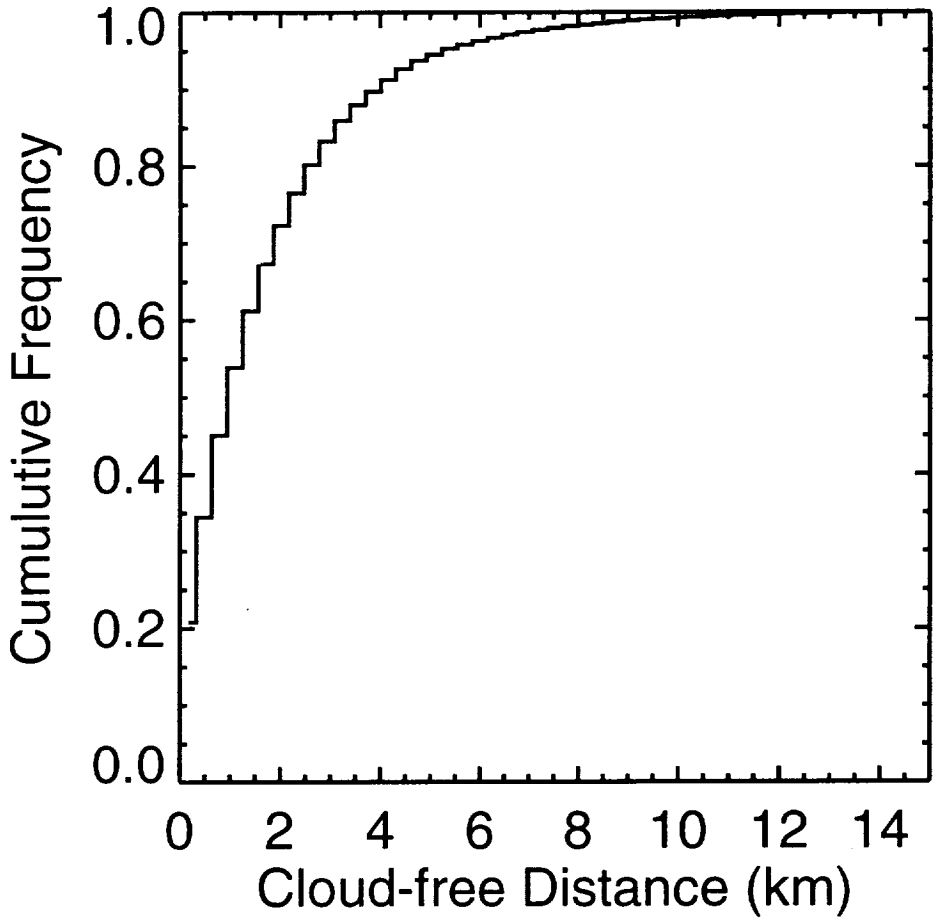
1.0
0.8
0.6
0.4
0.2
0.0
Cumulutive Frequency
0
2
4
6
8
10
12
14
Cloud-free Distance (km)

Fig 7

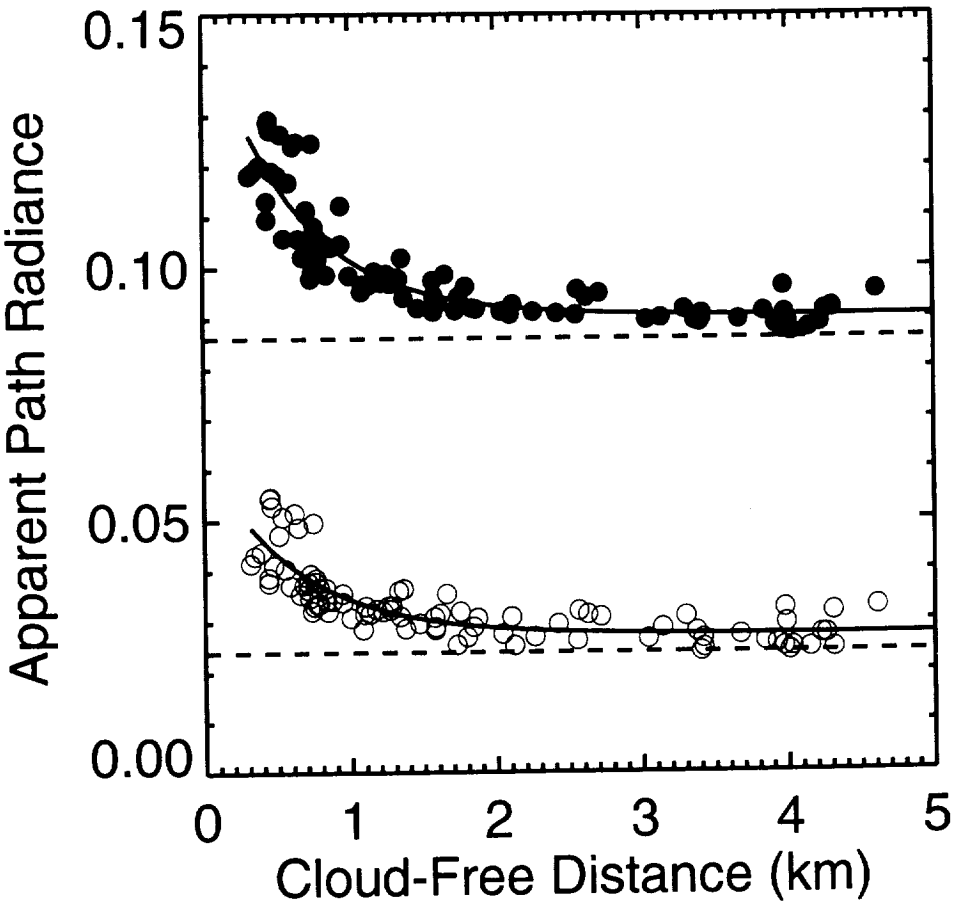
0.15
0.10
0.05
0.00
Apparent Path Radiance
0
1
2
3
4
5
Cloud-Free Distance (km)

Fig 2

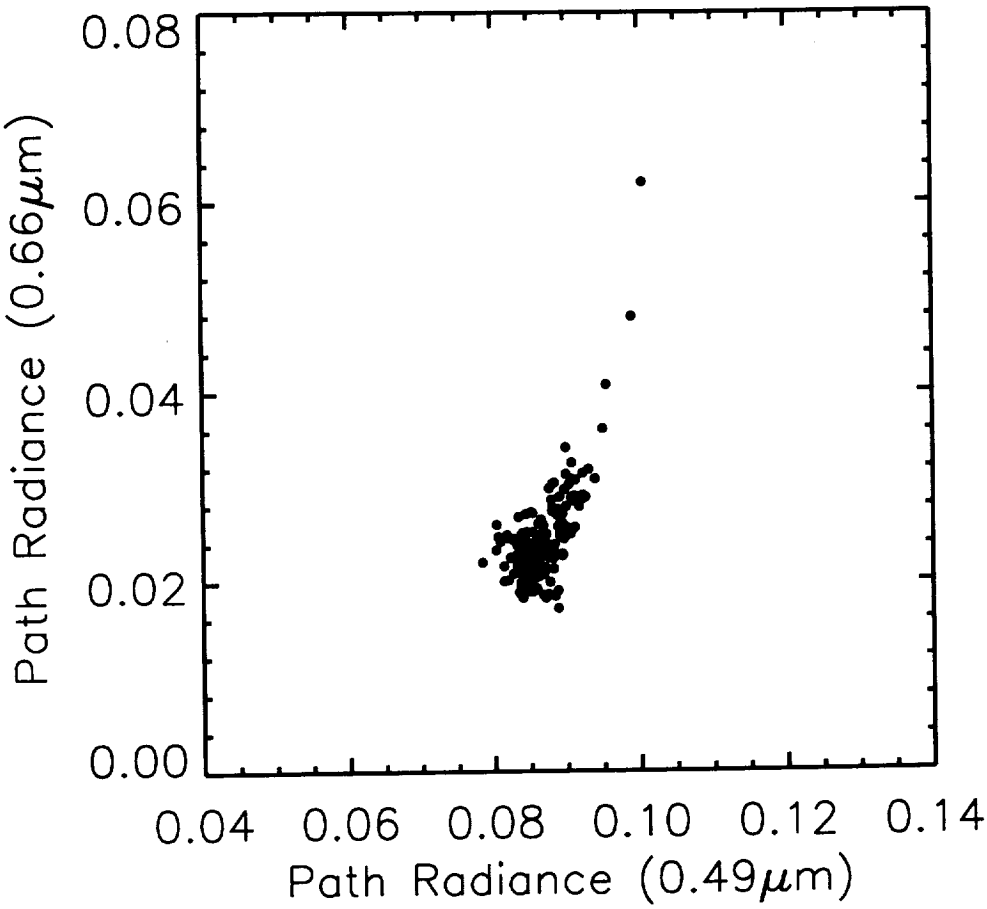
0.08
0.06
0.04
0.02
0.00
Path Radiance (0.66μm)
0.04
0.06
0.08
0.10
0.12
0.14
Path Radiance (0.49μm)

Fig 9